Journal of Materials Chemistry

Cite this: J. Mater. Chem., 2012, 22, 8634

www.rsc.org/materials

PAPER

Self-assembly of well-ordered whisker-like manganese oxide arrays on carbon fiber paper and its application as electrode material for supercapacitors†

Yongsong Luo,[abg] Jian Jiang,[a] Weiwei Zhou,[a] Huanping Yang,[a] Jingshan Luo,[a] Xiaoying Qi,[c] Hua Zhang,[c] Denis Y. W. Yu,[b] Chang Ming Li[de] and Ting Yu*[abf]

Received 7th December 2011, Accepted 28th February 2012
DOI: 10.1039/c2jm16419a

Self-assembled well-ordered whisker-like manganese dioxide (MnO_2) arrays on carbon fiber paper (MOWAs) were synthesized *via* a simple *in situ* redox replacement reaction between potassium permanganate ($KMnO_4$) and carbon fiber paper (CFP) without any other oxidant or reductant addition. The CFP serves as not only a sacrificial reductant and converts aqueous permanganate (MnO_4^-) to insoluble MnO_2 in this reaction, but also a substrate material and guarantees MnO_2 deposition on the surface. The electrochemical properties were examined by cyclic voltammograms (CV), galvanostatic charge/discharge, and electrochemical impedance spectroscopy (EIS) in a three-electrode cell. According to the CV results, the ordered MOWAs yield high-capacitance performance with specific capacitance up to 274.1 F g^{-1} and excellent long cycle-life property with 95% of its specific capacitance kept after 5000 cycles at the current density of 0.1 A g^{-1}. The high-performance hybrid composites result from a synergistic effect of large surface area and high degree of ordering of the ultrathin layer of MnO_2 nanowhisker arrays, combined with the flexible CFP substrate and can offer great promise in large-scale energy storage device applications.

Introduction

With the ever-increasing environmental problems and the up-coming depletion of fossil fuels, a great deal of research is being targeted towards developing sustainable and renewable clean energy production from the sun, the tides, the wind, and so on. Thus, efficient energy storage devices are needed to make the best of the electricity generated from these intermittent, renewable sources. Among the various energy storage systems, one such device is the electrochemical supercapacitor which has attracted a great deal of attention owing to its higher power density, longer cycle life than that of batteries, and higher energy density than that of conventional dielectric capacitors.[1–3] To bridge batteries and conventional capacitors, supercapacitors have been used in a variety of applications ranging from portable electronic devices, hybrid electrical vehicles, and large industrial scale power and energy management.[4,5] Depending on the charge storage mechanism as well as the active materials used, supercapacitors can be clarified into three types: electric double-layer capacitors (commonly using carbon-based materials with high surface area as electrodes),[1,4,6] redox capacitors or pseudocapacitors, which utilize transition metal oxides or conducting polymers as electrodes,[7,8] and hybrid electrochemical capacitors, which usually combine one battery-type faradaic electrode (as energy source) with the other capacitive electrode (as power source) in the same cell.[4] However, there are still drawbacks with these supercapacitor devices. The specific gravimetric and volumetric capacitances of carbon-based materials are far lower than those of transition metal oxides and conducting polymers, whereas transition metal oxides and conducting polymers are more expensive and exhibit poorer conductivity than carbon-based electrodes.[9–11] Therefore, designing an electrode with appropriate performance characteristics remains a significant challenge even today.

To enable supercapacitor devices for broad applications, a range of nanoscale building blocks as electrode materials have been investigated extensively.[12–15] Among a huge number of ways of designing materials, there has been growing interest in incorporating capacitive carbon materials with transition metal oxides. On one hand, conventional charge storage devices cannot provide the peak power needed without becoming too heavy or

[a]Division of Physics and Applied Physics, School of Physical and Mathematical Sciences, Nanyang Technological University, 637371, Singapore. E-mail: yuting@ntu.edu.sg
[b]Energy Research Institute at Nanyang Technological University, 639789, Singapore
[c]School of Materials Science and Engineering, Nanyang Technological University, 639798, Singapore
[d]Institute for Clean Energy and Advanced Materials, Southwest University, Chongqing 400700, P. R China
[e]Division of Bioengineering, School of Chemical and Biomedical Engineering, Nanyang Technological University, 637371, Singapore
[f]Department of Physics, Faculty of Science, National University of Singapore, 117542, Singapore
[g]School of Physics and Electronic Engineering, Xinyang Normal University, Xinyang 464000, P. R. China
† Electronic supplementary information (ESI) available. See DOI: 10.1039/c2jm16419a

bulky (many metal substrates have previously been used as current collectors, such as copper and aluminum), while the current developments are moving towards thin, light, cheap, and flexible current collectors.[15] On the other hand, MnO_2 has been envisaged as a representative of transition metal oxides and a promising supercapacitive material owing to its high specific capacitance, environmental compatibility, and cost effectiveness.[16–18] Thus far, much work has been reported on synthesis of MnO_2/carbon-based composite materials for supercapacitor applications.[16,19–24] For example, Zhou *et al.*[25] obtained mesoporous MnO_2 using mesoporous KIT-6 as template and the specific capacitance was 220 F g^{-1}. Yan *et al.*[26] synthesized graphene/MnO_2 composites by microwave irradiation and with specific capacitance as high as 310 F g^{-1}. Chen *et al.*[22] prepared graphene oxide/MnO_2 nanocomposites through a simple soft chemical route and the specific capacitance value of the sample was 197.2 F g^{-1}. Yu *et al.*[27] fabricated a hybrid graphene/MnO_2-based textile which yielded high-capacitance performance with specific capacitance up to 315 F g^{-1}. In addition, it is well known that the pseudocapacitive reactions occur on the metal oxide surface; and so only a large surface area or a very thin surface layer of oxide is capable of contributing to interfacial electrochemical reactions.[28] Moreover, a large pore size and high degree of ordering of mesoporous materials can further facilitate ion transfer.[29] Therefore, developing large surface area, high ordering degree, ultrathin layers, and combining flexible substrate electrode active materials are the crucial factors to address this issue for supercapacitors.

In this work, we demonstrate a facile method to prepare well-ordered whisker-like MnO_2 arrays on carbon fiber paper (CFP) serving as electrode materials for supercapacitors. First, CFP substrates offer many advantages for electrode devices since they are low-cost, flexible, lightweight, and disposable.[30,31] The intrinsic flexibility of thin-film materials is able to impart mechanical resilience, enable convenient roll-to-roll processing[32] and permit the fabrication of collapsible and portable devices.[33] Second, MnO_2 has been envisaged as a promising supercapacitive material owing to its high specific capacitance, environmental compatibility, and low cost. Third, the MnO_2 nanowhiskers form an ultrathin surface layer, which is capable of contributing to interfacial electrochemical reactions and provides a large electrode surface area. Moreover, one-dimensional (1D) whisker-like MnO_2 arrays grown on conductive substrates not only offer a good conducting pathway, but also can endure large volume changes as well as having good strain accommodation. Undoubtedly, these can contribute to improving the capacity and cycle life of supercapacitors.

Experimental section

Synthesis of MnO_2 nanowhisker arrays on carbon fiber paper (MOWAs)

All reagents used were of analytical grade and were used directly without any purification. In a typical synthesis procedure, 0.055 g of potassium permanganate ($KMnO_4$) was dissolved in deionized water (50 mL) under vigorous stirring for 30 min, forming a 7 mM $KMnO_4$ solution. Then, the fully dissolved solution was transferred into a Teflon-lined stainless steel autoclave. In the meantime, a piece of carbon paper made of randomly intertwined carbon fibers (NCBE, UK) was cut to a size of 1.5 × 4.0 cm. Finally, the reaction was kept at 160 °C for 3 h. After the autoclave was cooled to ambient temperature, the sample was removed, washed with distilled water, and dried at 60 °C to obtain MOWAs. For comparison, similar procedures were conducted to investigate the reaction at different $KMnO_4$ concentrations of 3, 5, and 15 mM, respectively.

Characterization

The phase purity of the products was characterized by X-ray powder diffraction (XRD) using a X-ray diffractometer with Cu-Kα radiation (λ = 1.5418 Å). Scanning electron microscopy (SEM) images and X-ray energy dispersive spectroscopy (EDS) analyses were obtained using a HITACHI S-4300 microscope (Japan). Transmission electron microscopy (TEM and HRTEM) observations were carried out on a JEOL JEM-2010 instrument in bright field and on a HRTEM JEM-2010FEF instrument (operated at 200 kV). The surface area was measured using a Micromeritics (NOVA 4200e) analyzer. The nitrogen adsorption and desorption isotherms were obtained at 77 K. The Brunauer–Emmett–Teller (BET) surface area was calculated from the linear part of the BET plot. Raman spectroscopy was carried out using a WITEC CRM200 Raman system equipped with a 532 nm laser source and 100× objective lens. X-ray photoelectron spectroscopy (XPS) spectra were measured on a PerkinElmer model PHI 5600 XPS system with a resolution of 0.3–0.5 eV from a monchromated aluminum anode X-ray source.

Electrochemical measurements

Electrochemical measurements were performed on an electrochemical workstation (CHI 760C, CH Instruments Inc., Shanghai) using a conventional three-electrode cell. The three-electrode cell configuration consisted of Pt as the counter electrode; Ag/AgCl as the reference electrode; and the MOWAs ($\approx 0.6 \times 2.5$ cm^2; CFP mass $\approx$ 6 mg; $MnO_2 \approx$ 1 mg) were directly used as the working electrode. A solution containing 1M Na_2SO_4 served as the electrolyte at room temperature. Cyclic voltammograms were recorded between 0 and 1.0 V (*vs.* Ag/AgCl) at various scan rates ranging from 10 to 200 mV s^{-1}. Galvanostatic charge/discharge testing was conducted between 0 and 1.0 V (*vs.* Ag/AgCl) at different current densities of 0.2–1 A g^{-1}. The electrochemical impedance spectroscopy (EIS) measurements were performed by applying an AC voltage with 5 mV amplitude in a frequency range from 0.1 Hz to 100 kHz. Areal and specific capacitances were calculated according to $C_a = I \times t/(\Delta V \times S)$ and $C_{sp} = I \times t/(\Delta V \times m)$, respectively, where I is the constant discharge current, t the discharging time, V the voltage drop upon discharging (excluding the IR drop), m the mass of MnO_2 nanowhisker arrays in the electrode material, and S the geometrical area of the electrode.

Results and discussion

The schematic illustration for the fabrication processes of MOWAs is shown in Fig. 1. MnO_2 can be produced on CFP surface by a green reaction between carbon and $KMnO_4$ in a pH neutral solution. The redox reaction is described in the following

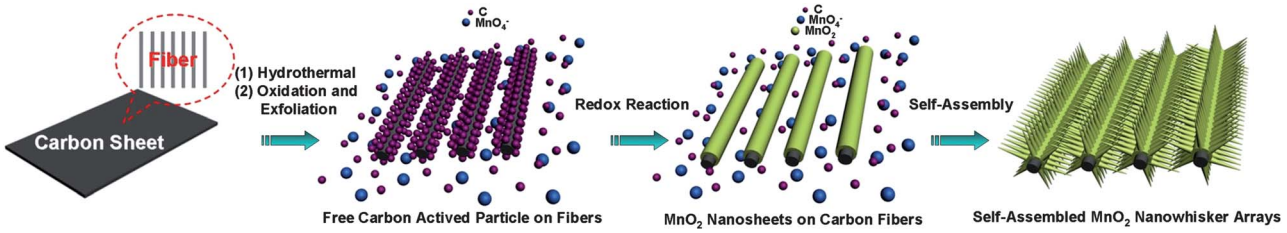

Fig. 1 Schematic illustration for the formation processes of the MOWAs.

equation ($4MnO_4^- + 3C + H_2O = 4MnO_2 + CO_3^{2-} + 2HCO_3^-$). Here, it is emphasized that the CFP serves as not only a sacrificial reductant by converting aqueous permanganate (MnO_4^-) to insoluble MnO_2, but also a substrate material. This guarantees that the formed whisker-like MnO_2 arrays, the active materials, can be directly loaded on the surface of CFP current collector, avoiding the use of any additive binders or conducting agents. The XRD confirms the presence of the birnessite-type MnO_2 (JCPDS 50-0866) with mixed crystalline and amorphous parts (Fig. S1†), where the (002) reflection peak of CFP has almost disappeared owing to producing a lot of amorphous structures. Broad and weak peaks are related to a poorly crystallized compound originating from the effect of amorphous carbon.

Fig. 2(a–c) show SEM images of as-synthesized well-ordered MOWAs at low, medium and high magnification, respectively. From the images, the high-yield production of whisker-like MnO_2 arrays can be clearly seen. Note that each whisker is made up of many ultrathin nanosheets, which are interconnected with each other, forming a highly porous surface morphology. Careful examination reveals that these whisker-like MnO_2 arrays are 3–5 μm in length and about 0.5 μm in diameter at the middle section. Almost all of them possess the same morphology and are projected from a common central axis zone. Fig. 2(d) shows the SEM image of the head of an individual MOWA, indicating that the carbon fiber is completely coated with well-ordered MnO_2 nanowhiskers. In order to probe the novel inner structure more clearly, we have studied the SEM images of cross-sectionally damaged MOWAs (See Fig. 2(e)), which further confirm, from inside to outside, the carbon fiber/MnO_2 core-whisker array hybrid structure. For comparison, the optical and low-magnification SEM images of the pristine CTP and products are presented as well, as shown in Fig. S2.† Raman spectroscopy was also used to investigate the samples of both CFP and MOWAs. In the Raman spectrum of CFP (Fig. 2(f)), the G band (1590 cm^{-1}) represents the in-plane bond-stretching motion of the pairs of C sp^2 atoms (the E_{2g} phonons), while the D band (1350 cm^{-1}) corresponds to breathing modes of rings or K-point phonons of A_{1g} symmetry.[34,35] Conversely, the MOWAs exhibit three distinct Raman peaks, at 507, 586, and 628 cm^{-1}, respectively, which are assigned to oxygen vibrations of the tunnel α-MnO_2 structure.[36] Control experiment studies also reveal that the final morphologies of the products are strongly affected by the reaction concentration of $KMnO_4$ solution (c), as displayed in Fig. S3.† For c = 3 mM, the large scale of carbon fiber/MnO_2 core-shell nanostructures (MOCSs) are observed (Fig. S3a†). When the c value increases from 3 to 5 mM, we find that the surfaces of MOCSs with few plumules are obtained (Fig. S3b†). When the c value reached 7 mM, the product consisted of highly ordered MOWAs (Fig. S3c†). Comparatively, at high concentrations ($c \geq 15$ mM), the product is mainly composed of ill-defined carbon fiber/MnO_2 core-shell nanostructures (I-MOCSs) (Fig. S3d†). As is mentioned above, the carbon substrate serves as a sacrificial reductant and converts aqueous MnO_4^- to insoluble MnO_2, in a certain concentration range for MnO_4^- ion solution; it could provide appropriate active carbon ions (as a reducing agent) for the self-assembly growth of whisker-like MnO_2 arrays. Therefore, the adjusting of the amount of $KMnO_4$ may result in different morphologies and sizes of the products.

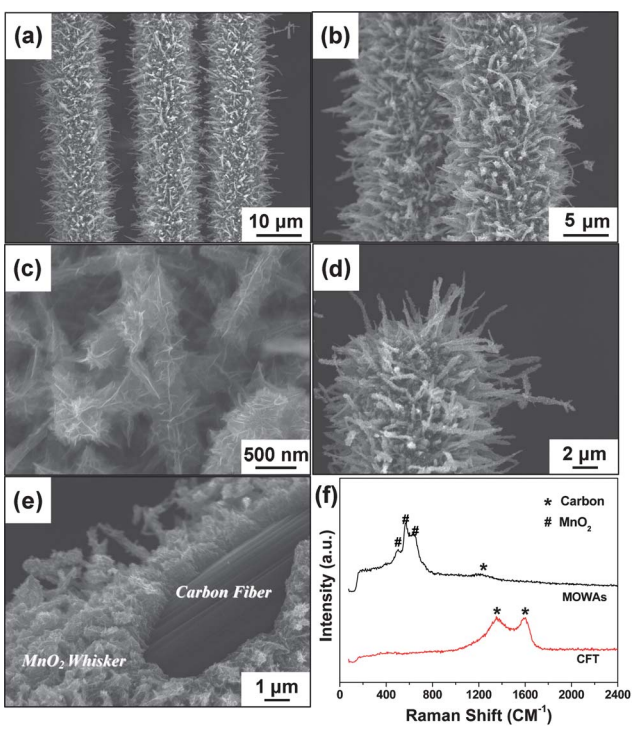

Fig. 2 (a–c) SEM images of MOWAs at various magnifications; (d) SEM image of the head of one MOWA; (e) SEM image of a cross-sectionally damaged MOWA; (f) Raman spectra of MOWAs. The spectrum of pure CFP is also shown for comparison.

To obtain more details of the microstructure of these MOWAs, the products were further investigated by TEM. Fig. 3(a) shows a typical TEM image of an individual nanostructure in which the whisker-like MnO_2 arrays uniformly cover the carbon fiber surface. The edge and center of the whiskers show strong brightness contrast, further confirming their ultrathin nature. The selected area electron diffraction (SAED) pattern was also performed for the area of MnO_2 nanowhiskers

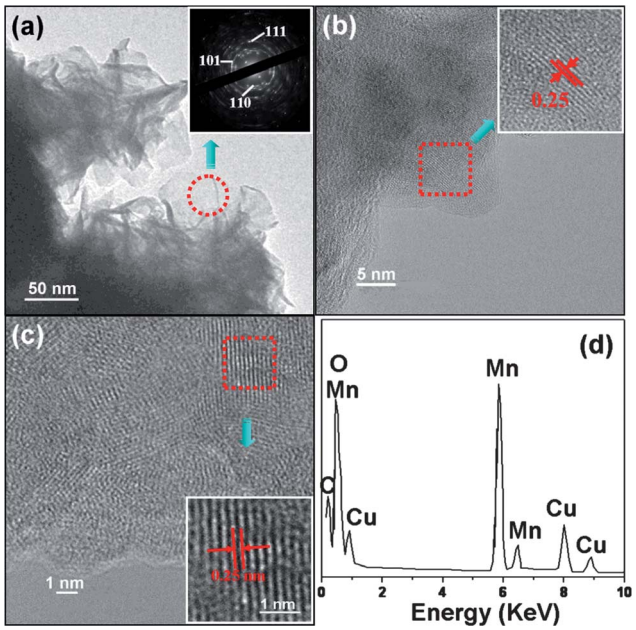

Fig. 3 (a) Low-magnification TEM image of MnO_2 nanowhiskers, the inset is the SAED result for the MnO_2 nanosheet; (b, c) HRTEM images of the MnO_2 sheet at different parts; (d) EDX spectra of the MOWAs.

circled in red (inset of Fig. 3(a)). The HRTEM image shown in Fig. 3(b) clearly reveals lattice fringes of 0.25 nm, corresponding to the (101) plane of birnessite-type MnO_2,[37] which is in agreement with the SAED result. Fig. 3(c) shows a typical TEM image of the edge of another MnO_2 nanowhisker, which presents the same crystal structure as shown in Fig. 3(b). The EDS result shown in Fig. 3(d) demonstrates that the as-prepared MOWAs contain C, Mn, O and Cu. The Cu-element is due to the Cu grid, and no other impurities are detected.

XPS studies were conducted in order to determine the presence of surface elements, their oxidation states, and the purity of as-synthesized products. The survey scan spectrum of the MOWAs in Fig. 4(a) shows that there are only three elements (Mn, O, and C) existing on the surface of the sample without evidence of any impurities. Fig. 4(b) gives the Mn 2p spectra of the MOWAs. Two peaks located at *ca.* 643.2 and 654.9 eV are observed with a spin-energy separation of 11.7 eV, which can be attributed to the Mn $2p_{3/2}$ and Mn $2p_{1/2}$ binding energies, respectively.[38] The deconvolution peaks (Fig. 4(c)) of the O 1s spectrum are resolved into four components, centered at 530, 531, 532, and 533.7 eV, respectively. The low binding energy component observed at 530 eV is attributed to the O^{2-} forming oxide with manganese elements (Mn–O–Mn), while the band at 531 eV corresponds to hydroxide (Mn–O–H).[38] The later two peaks are assigned to C–O (or O–C=O) and H_2O.[39–41] Herein, this result clearly indicates that a certain degree of oxidation occurred during the preparation of MOWAs. It is well-known that potassium permanganate ($KMnO_4$) is a strong oxidant. Some carboxylic acid groups as well as other oxygenated functional groups can be expected on the carbon fibers surface after immersing the carbon fibers in $KMnO_4$ solution at elevated temperature. The XPS spectrum of C 1s core-level from CFP (Fig. 4(d)) is also decomposed into four peaks at 284.8, 286.4, 288, and 290 eV, respectively.[42] These components can be assigned to C from non-oxygenated carbon (CC), COC/COH, a carbonyl group (CO), and a COOH group, respectively. The specific surface area of the MOWAs was determined by nitrogen adsorption–desorption measurement at 77 K. Fig. S4† shows the nitrogen adsorption–desorption isotherms that could be classified as type III by referring to BDDT.[43] The specific surface area calculated by the Brunauer–Emmett–Teller (BET) method is *ca.* 55.7 $m^2\ g^{-1}$ for the MOWAs. This is attributed to the fact that the MOWAs have a whisker-like structure growing radially from the fiber core. Barrett–Joyner–Halenda (BJH) calculations for the pore size distribution, derived from desorption data, reveal a narrow distribution for the whisker-like nanostructures centered at 2 nm (inset of Fig. S4†). Such nanostructure with much higher surface area will undoubtedly have good performance for electrochemical supercapacitors.

To demonstrate the advantage of this unique structure and further explore the potential applications in supercapacitors, electrochemical tests were carried out in a three-electrode configuration with a Pt plate counter electrode and an Ag/AgCl reference electrode in 1 M Na_2SO_4 aqueous electrolyte solution. Fig. 5(a) shows the cyclic voltammograms (CVs) of a whisker-like MnO_2 arrays electrode at scan rates of 10–200 mV s^{-1}. Although the shapes of the CV curves deviate from ideal rectangular shape, the areas surrounded by the CV curves are not significantly influenced by the change in scan rates, implying good rate capability of the sample. For comparison, the CV of the pristine CFP, MOCSs, and I-MOCSs at 50 mV s^{-1} are also shown in Fig. 5(b). It is noted that the current density of the MOWAs at the same scan rate is higher than that for other electrode materials. The significant increase of the CV integrated area suggests that the whisker-like MnO_2 arrays have a much higher specific capacitance, as will be discussed. Therefore, the excellent electrochemical capability of MOWAs may be attributed to their unique microstructures, which can contribute to the rapid intercalation of cations (Na^+) in the electrode during reduction and deintercalation upon oxidation.[38,44] The MOWAs were also characterized using galvanostatic charge/discharge measurements, as shown in Fig. 5(c). It can be seen that all the curves are highly linear and symmetrical at various current densities from 200 to 1000 mA g^{-1}. This implies that the electrode has excellent electrochemical reversibility and charge–discharge properties. Furthermore, the specific capacitance can be calculated from the discharge curves according to the above-mentioned equations. On the basis of the above results, the specific capacitance of the MOWAs at 100, 200, 300, 500, and 1000 mA g^{-1} is 274.1, 171.6, 150.5, 106.4, and 54 F g^{-1}, respectively. About 50.8% of *C* was retained when the current density increased from 500 to 1000 mA g^{-1}. These results can be ascribed to the discrepant insertion–deinsertion behaviors of cations (Na^+) from the electrolyte to MnO_2.[45] It is emphasized that the specific capacitance is calculated according to the mass of the whisker-like MnO_2, and carbon materials are not included for this calculation. The specific capacitance (*C*) based on the mass of the whisker-like MnO_2 arrays *versus* current density plots is also shown in Fig. 5(d).

The cycle stability of supercapacitors is a crucial parameter for their practical applications. The long-term stability of the electrodes was examined at 100 mA g^{-1} and the results are shown in

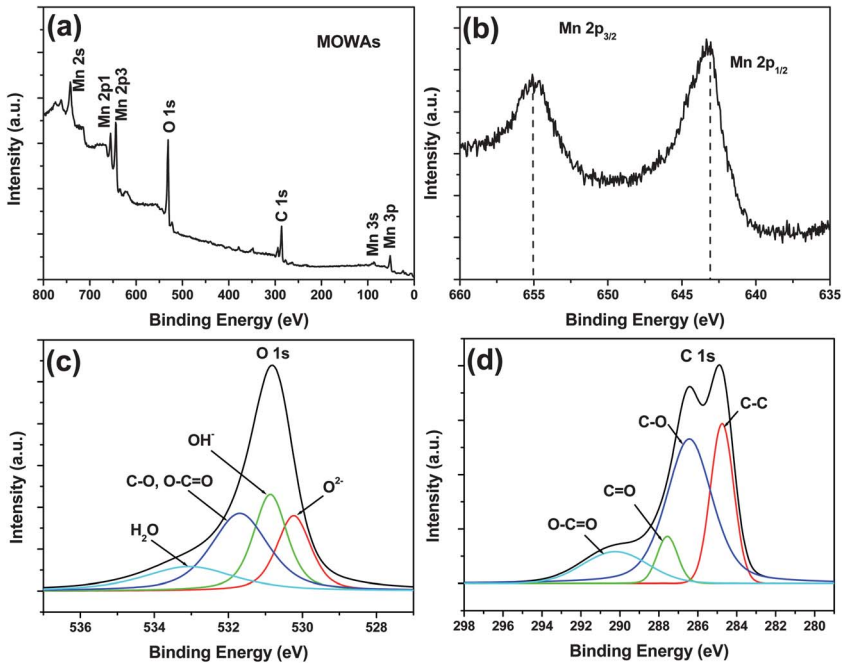

Fig. 4 (a) Survey XPS spectrum; (b) Mn 2p XPS spectrum; (c) O 1s and (d) C 1s XPS spectra for the MOWAs.

Fig. 6(a). It is found that the MOWAs electrode capacitance retention is more than about 95% of the initial value after 5000 cycles, while that of the MOCSs also retained good cycle stability performance. The MOWAs electrode exhibits a good long-term electrochemical stability, which is evident from the very stable charge/discharge curves for the last 15 cycles (Fig. 6(b)). The results indicate that the charge curves are still quite symmetric to their corresponding discharge counterparts, showing no significant structural change of the MOWAs electrode during the charge/discharge processes. As is known, the redox/pseudocapacitive reactions happen on the surface of transition metal oxides; only a thin surface layer of oxides can participate in this reaction. The MOWAs consist of small MnO_2 sheets with well separated surfaces, making them almost fully available to the

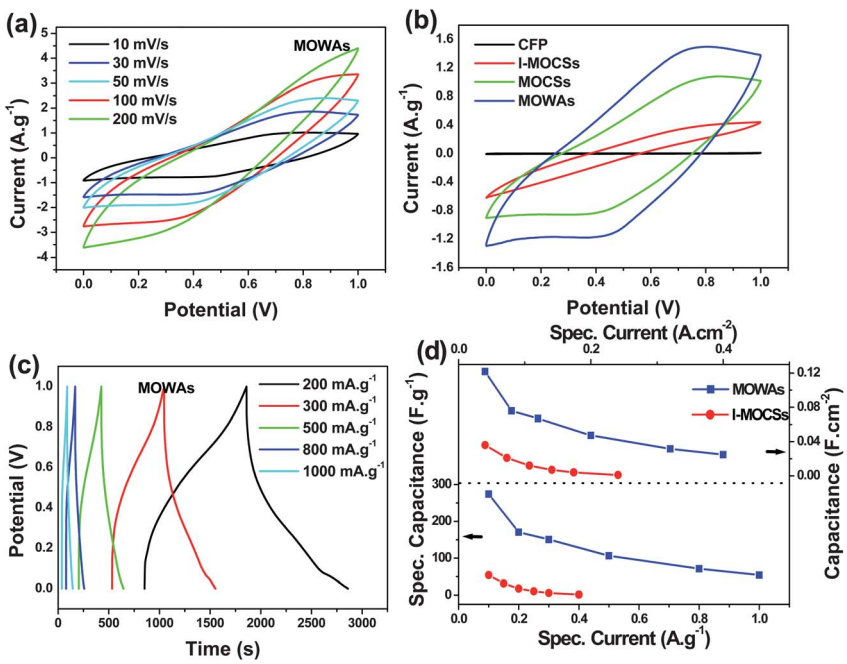

Fig. 5 (a) Cyclic voltammograms of MOWAs at different scan rates; (b) Cyclic voltammograms of the different electrode materials at 50 mV s^{-1}; (c) Charge/discharge curves of MOWAs at various current densities; (d) Current density dependence of the areal capacitance (above) and specific capacitance (below) of MOWAs.

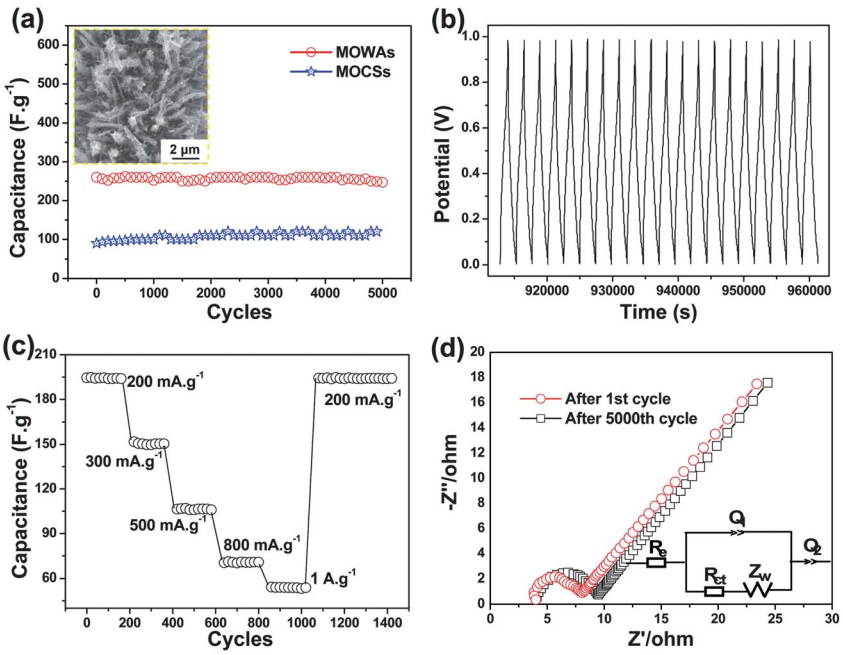

Fig. 6 (a) Cycling performance of the MOWAs; (b) The charge/discharge curves of the last 15 cycles for the MOWAs; (c) Cycling stability of the MOWAs at progressively various current densities; (d) Equivalent circuit, and electrochemical impedance spectra after 1st and 5000th cycles.

Na^+ in the electrolyte.[22,46] The entirely exposed nanosheet edges can also facilitate the fast Na^+ intercalation into the layered structure, thus enhancing the electrochemical kinetics. Besides, the CFP in the hybrid materials can provide not only double-layer capacitance to the overall energy storage but also fast electronic transfer channels to improve the electrochemical performance. Furthermore, the directly grown array can ensure good mechanical adhesion and electrical connection to the current collector,[47] avoiding the use of polymer binders and conducting additives, which generally increase the series resistance and the deterioration of capacitance during redox reactions. Another key advantage of this electrode structure is its robust mechanical stability, rather than being stiff or rigid, owing to the nature of carbon fiber materials. The MOWAs nanostructures are well maintained and overall preserved with little structural deformation after 5000 cycles as also verified in the inset of Fig. 6(a). For a better understanding of the synergistic effect in this electrode design, the cycling performance of the MOWAs at progressively increased current density was recorded in Fig. 6(c). During the first 200 cycles with a charge/discharge density of 200 mA g^{-1}, the hybrid structure shows a cycle stability performance of 194 F g^{-1}. In the following 800 cycles, the charge/discharge rate changes successively. The hybrid structure always demonstrates stable capacitance even when suffering from a sudden change of the current delivery. After 1000 cycles, with the current rate being again decreased back to 200 mA g^{-1} for another 400 cycles, a capacitance of ~193 F g^{-1} can be recovered and without noticeable decrease, which demonstrates the hybrid structure has excellent rate performance and cyclability. For comparison, the capacitive performances of different MnO_2 nanocomposites have been summarized in Table S1.†

EIS analysis has been recognized as one of the principal methods to examine the fundamental behavior of electrode materials for supercapacitors. To further understand the advantage of this electrode material device, impedance spectra of the MOWAs were measured at open circuit potential with an AC perturbation of 5 mV in the frequency range from 0.1 Hz to 100 kHz. Fig. 6(d) shows that the resulting Nyquist plot exhibits two distinct parts including an arc in the middle- and high-frequency region, and a sloped line in the low-frequency region. At lower frequencies, the straight line has a finite slope which represents the diffusive behavior changes of the electrolyte in the electrode pores. The arc in the high frequency range is associated with the surface properties of the MOWAs electrode and corresponds to the charge transfer resistance. The measured impedance spectra were analyzed using the complex nonlinear least-squares fitting method on the basis of the equivalent circuit, which is also given in the inset of Fig. 6(d), where R_e is the internal resistance, Q_1 and Q_2 are the double-layer capacitance and pseudocapacitance, respectively, R_{ct} is the charge transfer resistance, and Z_w is the Warburg impedance.[48] An obvious difference between the two spectra is that R_{ct} increases from 4.2 to 5.1 Ω after 5000 cycles. In the low frequency region, the Nyquist diagram shows a 45° slope relating closely to that of the Warburg impedance which corresponds to the porous nature of nano-MnO_2 and does not change after 5000 cycles.[49,50] All of these are probably attributed to the good contact between the current-collector and whisker arrays, indicating that the MOWAs are a promising supercapacitor electrode material.

Conclusions

In summary, we have demonstrated that well-ordered MOWAs nancomposites can be synthesized *via* a novel and facile *in situ* redox replacement reaction between $KMnO_4$ and CFP without

any other oxidant or reductant addition. The CFP serves as not only a sacrificial reductant and converts aqueous permanganate (MnO_4^-) to insoluble MnO_2 in this reaction, but also a substrate material and guarantees MnO_2 be deposited on the surface. The integration of CFP and the whisker-like MnO_2 crystals enables such hybrids to possess excellent electrochemical properties that are very useful and critical for electrode materials for supercapacitors. The large surface area, high ordering degree and ultrathin layer of MnO_2 nanowhisker arrays combined with the flexible CFP substrate can offer great promise in large-scale energy storage device applications.

Acknowledgements

This work is supported by the Singapore National Research Foundation under NRF RF Award No. NRF-RF2010-07, MOE Tier 2 MOE2009-T2-1-037 and CRP Award No.: NRF-CRP4-2008-03.

References

1 L. L. Zhang and X. S. Zhao, *Chem. Soc. Rev.*, 2009, **38**, 2520.
2 X. S. Fang, L. M. Wu and L. F. Hu, *Adv. Mater.*, 2011, **23**, 585.
3 Y. Y. Lu, F. Zhang, Y. Q. Dou, Y. P. Zhai, J. X. Wang, H. J. Liu, Y. Y. Xia, B. Tu and D. Y. Zhao, *J. Mater. Chem.*, 2012, **22**, 93.
4 P. Simon and Y. Gogotsi, *Nat. Mater.*, 2008, **7**, 845.
5 J. R. Miller and P. Simon, *Science*, 2008, **321**, 651.
6 J. P. Liu, Y. Y. Li, X. T. Huang, R. M. Ding, Y. Y. Hu, J. Jiang and L. Liao, *J. Mater. Chem.*, 2009, **19**, 1859.
7 L. Zhao, Y. S. Hu, H. Li, Z. X. Wang and L. Q. Chen, *Adv. Mater.*, 2011, **23**, 1385.
8 J. Huang, B. G. Sumpter and V. Meunier, *Angew. Chem., Int. Ed.*, 2008, **47**, 520.
9 Y. Wang, C. Y. Foo, T. K. Hoo, M. Ng and J. Lin, *Chem.–Eur. J.*, 2010, **16**, 3598.
10 L. Z. Fan, Y. S. Hu, J. Maier, P. Adelhelm, B. Smarsly and M. Antoniett, *Adv. Funct. Mater.*, 2007, **17**, 3083.
11 H. L. Wang, Q. M. Gao and L. Jiang, *Small*, 2011, **7**, 2454.
12 X. S. Fang, T. Y. Zhai, U. K. Gautam, L. Li, L. M. Wu, Y. Bando and D. Golberg, *Prog. Mater. Sci.*, 2011, **56**, 175.
13 Z. J. Fan, J. Yan, T. Wei, L. J. Zhi, G. Q. Ning, T. Y. Li and F. Wei, *Adv. Funct. Mater.*, 2011, **21**, 2366.
14 X. S. Fang, L. F. Hu, K. F. Huo, B. Gao, L. J. Zhao, M. Y. Liao, P. K. Chu, Y. Bando and D. Golberg, *Adv. Funct. Mater.*, 2011, **21**, 3907.
15 M. Kaempgen, C. K. Chan, J. Ma, Y. Cui and G. Gruner, *Nano Lett.*, 2009, **9**, 1872.
16 S. B. Ma, K. W. Nam, W. S. Yoon, X. Q. Yang, K. Y. Ahn, K. H. Oh and K. B. Kim, *J. Power Sources*, 2008, **178**, 483.
17 S. Komaba, A. Ogata and T. Tsuchikawa, *Electrochem. Commun.*, 2008, **10**, 1435.
18 G. An, P. Yu, M. Xiao, Z. Liu, Z. Miao, K. Ding and L. Mao, *Nanotechnology*, 2008, **19**, 275709.
19 Z. S. Wu, W. C. Ren, D. W. Wang, F. Li, B. L. Liu and H. M. Cheng, *ACS Nano*, 2010, **4**, 5835.
20 J. K. Chang, C. T. Lin and W. T. Tsai, *Electrochem. Commun.*, 2004, **6**, 666.
21 S. R. Sivakkumar, J. M. Ko, D. Y. Kim, B. C. Kim and G. G. Wallace, *Electrochim. Acta*, 2007, **52**, 7377.
22 S. Chen, J. W. Zhu, X. D. Wu, Q. F. Han and X. Wang, *ACS Nano*, 2010, **4**, 2822.
23 S. W. Lee, J. Kim, S. Chen, P. T. Hammond and Y. Shao-Horn, *ACS Nano*, 2010, **4**, 3889.
24 L. Hu, M. Pasta, F. L. Mantia, L. Cui, S. Jeong, H. D. Deshazer, J. W. Choi, S. M. Han and Y. Cui, *Nano Lett.*, 2010, **10**, 708.
25 Q. Zhou, X. Li, Y. G. Li, B. Z. Tian, D. Y. Zhao and Z. Y. Jiang, *Chin. J. Chem.*, 2006, **24**, 835.
26 J. Yan, Z. J. Fan, T. Wei, W. Z. Qian, M. L. Zhang and F. Wei, *Carbon*, 2010, **48**, 3825.
27 G. H. Yu, L. B. Hu, M. Vosgueritchian, H. L. Wang, X. Xie, J. R. McDonough, X. Cui, Y. Cui and Z. N. Bao, *Nano Lett.*, 2011, **11**, 2905.
28 S. B. Ma, K. Y. Ahn, E. S. Lee, K. H. Oh and K. B. Kim, *Carbon*, 2007, **45**, 375.
29 M. B. Zheng, J. Cao, S. T. Liao, J. S. Liu, H. Q. Chen, Y. Zhao, W. J. Dai, G. B. Ji, J. M. Cao and J. Tao, *J. Phys. Chem. C*, 2009, **113**, 3887.
30 A. C. Siegel, S. T. Phillips, M. D. Dickey, N. Lu, Z. Suo and G. M. Whitesides, *Adv. Funct. Mater.*, 2010, **20**, 28.
31 A. W. Martinez, S. T. Phillips, M. J. Butte and G. M. Whitesides, *Angew. Chem., Int. Ed.*, 2007, **46**, 1318.
32 F. C. Krebs, T. Tromholt and M. Jorgensen, *Nanoscale*, 2010, **2**, 873.
33 Y. G. Sun and J. A. Rogers, *Adv. Mater.*, 2007, **19**, 1897.
34 A. C. Ferrari and J. Robertson, *Philos. Trans. R. Soc. London, Ser. A*, 2004, **362**, 2477.
35 L. G. Cancado, M. A. Pimenta, B. R. A. Neves, M. S. S. Dantas and A. Jorio, *Phys. Rev. Lett.*, 2004, **93**, 247401.
36 C. M. Julien, M. Massot and C. Poinsignon, *Spectrochim. Acta, Part A*, 2004, **60**, 689.
37 W. Xiao, D. L. Wang and X. W. Lou, *J. Phys. Chem. C*, 2010, **114**, 1694.
38 M. Toupin, T. Brousse and D. Belanger, *Chem. Mater.*, 2004, **16**, 3184.
39 G. Bhargava, I. Gouzman, C. M. Chun, T. A. Ramanarayanan and S. L. Bernasek, *Appl. Surf. Sci.*, 2007, **253**, 4322.
40 T. Yamashita and P. Hayes, *Appl. Surf. Sci.*, 2008, **254**, 2441.
41 G. K. Pradhan and K. M. Parida, *ACS Appl. Mater. Interfaces*, 2011, **3**, 317.
42 L. Tang, Y. Wang, Y. Li, H. Feng, J. Lu and J. Li, *Adv. Funct. Mater.*, 2009, **19**, 2782.
43 K. S. W. Sing, D. H. Everett, R. A. W. Haul, L. Moscou, R. A. Pierotti, J. Roquerol and T. Siemieniewska, *Pure Appl. Chem.*, 1985, **57**, 603.
44 V. Subramanian, H. W. Zhu and B. Q. Wei, *J. Power Sources*, 2006, **159**, 361.
45 V. Subramanian, H. Zhu, R. Vajtai, P. M. Ajayan and B. Wei, *J. Phys. Chem. B*, 2005, **109**, 20207.
46 J. P. Liu, J. Jiang, C. W. Cheng, H. X. Li, J. X. Zhang, H. Gong and H. J. Fan, *Adv. Mater.*, 2011, **23**, 2076.
47 J. Jiang, Y. Y. Li, J. P. Liu and X. T. Huang, *Nanoscale*, 2011, **3**, 45–58.
48 J. J. Yoo, K. Balakrishnan, J. S. Huang, V. Meunier, B. G. Sumpter, A. Srivastava, M. Conway, A. L. M. Reddy, J. Yu, R. Vajtai and P. M. Ajayan, *Nano Lett.*, 2011, **11**, 1423.
49 N. Shinji, W. Hajime and F. Naoji, *Electrochim. Acta*, 2003, **48**, 749.
50 Y. Chen, M. L. Zhang and Z. H. Shi, *J. Electrochem. Soc.*, 2005, **152**, A1272.

